Supplement of Atmos. Chem. Phys., 17, 7567–7579, 2017
https://doi.org/10.5194/acp-17-7567-2017-supplement

Atmospheric Chemistry and Physics
Open Access
EGU

Supplement of

Observations of bromine monoxide transport in the Arctic sustained on aerosol particles

Peter K. Peterson et al.

Correspondence to: Kerri A. Pratt (prattka@umich.edu)

Supporting Information (SI)

This supplement contains additional details on methods used in this study.

Profile Retrieval from Limb Viewing DOAS Measurements

Limb viewing measurements are commonly used to generate vertical profiles of trace gases when the aircraft is ascending or descending Prados-Roman et al. (2011). A full description of the techniques used in both the initial DOAS fitting (General et al., 2014) and profile retrievals (Frieß et al., 2011) has been published previously, and thus the profile retrievals are only briefly described here.

Vertical profiles of BrO were retrieved on the ascent after takeoff from the Barrow airport (Fig. S1), as well as the final descent prior to landing at the Barrow airport. Differential slant column densities (dSCDs) were determined for BrO and O_4 using the DOAS technique (Platt and Stutz, 2008) implemented using DOASIS software (Kraus, 2006). The reference spectrum for the DOAS fitting was taken prior to takeoff using a sand blasted teflon plate to direct sunlight to the limb viewing telescope. Full details of the DOAS fitting and absorption cross sections used are given in General et al. (2014). These dSCDs were then used as input in a two step optimal estimation procedure (Frieß et al., 2011) to retrieve profiles of aerosol particle extinction and BrO in the lowest 2 km of the boundary layer. In this case, optimal estimation uses a radiative transfer model to model dSCD measurements based on an input vertical profile of either aerosol particle extinction or BrO every 100 m. This input profile is then varied to achieve agreement between the measured dSCDs and those modeled using the radiative transfer model SCIATRAN (Rozanov et al., 2005), which serves as the forward model. First, because O_4 has a known vertical profile, O_4 dSCDs, which strongly depend on visibility and light scattering, were used to retrieve a vertical profile of aerosol particle extinction every 100m from the ground to 2 km (Frieß et al., 2006). Measurement data alone are not sufficient to determine the profile, so an a priori profile is required to fully constrain the retrieved profile. For both the aerosol particle extinction and the BrO retrievals, the profiles retrieved from the ground based measurements at Barrow were used as an a priori. This retrieved aerosol extinction profile was then used as an additional input to SCIATRAN for the BrO profile retrieval, which is retrieved in a similar fashion (Frieß et al., 2011).

The sensitivity of the retrieved profiles to the true profile is described by the averaging kernel matrix (Rodgers, 2000) (Fig. S2). The trace of this matrix is referred to as the degrees of freedom for signal (DOFS) and can be thought of as the number of pieces of information that are retrieved. An ideal averaging kernel matrix would be the identity matrix, with DOFS equal to the number of parameters (aerosol particle extinction or BrO molar ratios in each 100m layer), implying every parameter is fully constrained by the measurements. However, in practice, not every parameter is fully constrained by observational data, leading to non-zero off-diagonal elements in the averaging kernel matrix, indicating decreased sensitivity to individual layers. For the ascent profile retrievals, limb viewing dSCDs from 202 to 907m were used as input into the retrieval. Because there are no measurements below 200m, the profiles on takeoff are poorly constrained at lower altitudes leading to low degrees of freedom (Fig. S2) and larger errors (Fig. S3). The error has two main components, one arises from errors associated with the dSCD measurements themselves, and the other is so-called "smoothing error", which arises from the fact that the retrieved profile represents a smoothed version of the true profile rather than the actual profile. Despite the large error bars, the retrieved profiles on ascent is consistent with ground based measurements shown in the main text, which have maximum sensitivity near the surface and showed there was minimal BrO near the surface and the majority of the BrO was aloft. Additionally, the retrieval averaging kernels indicate the retrieval around the plume altitude was well constrained by measurement data. For descent profile retrievals, dSCDs from 1039 - 72 m were used as retrieval input. Because these measurements cover a greater altitude range, they have a much larger information content which is reflected in the increased DOFS.

Chemical Ionization Mass Spectrometry

The sampling inlet and CIMS are described by Peterson et al. (2015). Briefly, the outer portion of the inlet was a 4.6 cm ID aluminum pipe that extended $\sim$9 cm beyond the wall of the sampling building. A blower was used to pull a total flow of $\sim$300 lpm through 33 cm of the aluminum pipe. 7.4 lpm of this flow was sampled into a 30°C heated 25 cm, 0.65 cm ID PFA path that included a custom three-way valve for calibration and background measurements. Following the valve, 2.0 lpm entered the CIMS flow reactor , where $I(H_2O)_n^-$ reagent ions were produced by passing 1.7 lpm of 5 ppm CH_3I in N_2 through a ^{210}Po

ionizer and mixed in the flow reactor with vapor vapor in N_2 (0.12 lpm) from a room temperature ($\sim$20°C) 1 L bubbler. Each mass was monitored for 500 ms with a 5% duty cycle. Background measurements were performed every 15 min by passing the air flow through a glass wool scrubber. Br_2 calibration was performed every 2 h by adding Br_2, from a permeation source, in a 21 mL min^{-1} N_2 flow, to the ambient sample air flow. A relative sensitivity of 0.47 for BrO (mass 224) relative to Br_2 (mass 287) was used for calibration of BrO (Liao et al., 2011); for calibration of HOBr (mass 225), a relative sensitivity of 0.5 relative to Br_2 (mass 287) was used (Liao et al., 2012). For March 11-13, 2012, the 3σ limits of detection for Br_2 (mass 287), BrO (mass 224), and HOBr (mass 225) were calculated to be 3.3 pmol mol^{-1}, 2.8 pmol mol^{-1}, and 3.3 pmol mol^{-1}, respectively, on average, for a 2.8 s integration period (corresponding to 1 min. of CIMS measurements). Since the variance in the background is likely due to counting statistics (Liao et al., 2011), the limits of detection for 1 h averaging are reported in the main text.

Aerosol Inlet Transmission Efficiency Calculations

The inlet sampling characteristics are dependent on the aspiration characteristics of the inlet located at the front end of the aircraft, the particle transport characteristics through the inlet tubing, and the aspiration efficiency of the Grimm sample tube pick-off. The aspiration efficiency of the inlet was determined using computation fluid dynamics to model the flow field around the inlet while the aircraft was in flight. Downstream of the entrance region, particle transport losses in tubing within the aircraft leading to the GRIMM were calculated using the empirical equations for sedimentation loss (Heyder and Gebhart, 1977), diffusional loss (Gormly and Kennedy, 1948), and turbulent inertial loss (Kulkarni et al., 2005) in the different sections of the inlet tubing. Particles were assumed to be well mixed in the sample flow and electrostatic losses were not considered. The optical particle counter (Grimm Inc. Model 1.109) sampled air flow anisokinetically from the main inlet tubing. We calculated this anisokinetic enhancement based on the empirical equation of Belyaev and Levin (Belyaev and Levin, 1974). The peak enhancement occurs just above one micron with particle counts in the 1-1.3 micron size bin being enhanced by a factor of 1.8. The efficiency drops below 35 percent at 4 microns, and thus particles larger than this are not considered in this work.

Additional Discussion of HYSPLIT Backward Air Mass Trajectories

Figure S5 shows the T850 temperature map for three days prior to the plume observation. Three of the ensemble trajectories are from Northern Siberia, while the bulk of the trajectories originate over the North Pole. These trajectories potentially indicate mixing of air masses occurring as the event is transported to Utqiagvik. The modeled vertical motion of the air mass upward from the surface is shown in Fig. S6. The vertical motion becomes more uncertain further back in the trajectory, however the omega field data shown in the manuscript are also consistent with upward motion of the observed air mass prior to observation by the aircraft.

Diffusion Limitation Calculations

Because of the low number concentrations corresponding to the observed supermicron particle surface areas, diffusion of HOBr to the particle surface could potentially limit the rate of the heterogeneous reaction of HOBr required for production of Br_2. These limitations are estimated in Fig. S7a, which shows the reduction in the uptake coefficient (γ_{eff}) as a function of particle diameter (Tang et al., 2014). Using this reduced uptake coefficient and assuming γ=0.6 (Wachsmuth et al., 2002), we then calculated the effective heterogeneous reaction rate, shown as a function of surface area concentration for 1-4 micron particles in Fig. S7b. Efficient recycling requires that this heterogeneous chemistry proceeds at a faster rate than concurrently occurring HOBr photolysis, which was calculated using data from the 2009 OASIS Barrow field campaign (Thompson et al., 2015). The calculated reaction rates suggest the observed supermicron aerosol particle surface area concentrations, which represent a lower bound on the total available surface area for heterogeneous reactions, are likely sufficient to sustain heterogeneous recycling.

References

Belyaev, S. and Levin, L.: Techniques for collection of representative aerosol samples, Journal of Aerosol Science, 5, 325–338, doi:10.1016/0021-8502(74)90130-X, http://linkinghub.elsevier.com/retrieve/pii/002185027490130X, 1974.

Frieß, U., Monks, P. S., Remedios, J. J., Rozanov, A., Sinreich, R., Wagner, T., and Platt, U.: MAX-DOAS O 4 measurements: A new technique to derive information on atmospheric aerosols: 2. Modeling studies, Journal of Geophysical Research, 111, D14 203, doi:10.1029/2005JD006618, http://www.agu.org/pubs/crossref/2006/2005JD006618.shtml, 2006.

Frieß, U., Sihler, H., Sander, R., Pöhler, D., Yilmaz, S., and Platt, U.: The vertical distribution of BrO and aerosols in the Arctic: Measurements by active and passive differential optical absorption spectroscopy, Journal of Geophysical Research, 116, doi:10.1029/2011JD015938, http://www.agu.org/pubs/crossref/2011/2011JD015938.shtml, 2011.

General, S., Pöhler, D., Sihler, H., Bobrowski, N., Frieß, U., Zielcke, J., Horbanski, M., Shepson, P. B., Stirm, B. H., Simpson, W. R., Weber, K., Fischer, C., and Platt, U.: The Heidelberg Airborne Imaging DOAS Instrument (HAIDI) – a novel imaging DOAS device for 2-D and 3-D imaging of trace gases and aerosols, Atmospheric Measurement Techniques, 7, 3459–3485, doi:10.5194/amt-7-3459-2014, http://www.atmos-meas-tech.net/7/3459/2014/amt-7-3459-2014.html, 2014.

Gormly, P. and Kennedy, M.: Diffusion from a Stream Flowing through a Cylindrical Tube, Proceedings of the Royal Irish Academy. Section A: Mathematical and Physical Sciences, 52, 163–169, http://www.jstor.org/stable/20488498, 1948.

Heyder, J. and Gebhart, J.: Gravitational deposition of particles from laminar aerosol flow through inclined circular tubes, Journal of Aerosol Science, 8, 289–295, doi:10.1016/0021-8502(77)90048-9, http://linkinghub.elsevier.com/retrieve/pii/0021850277900489, 1977.

Kraus, S.: DOASIS –A Framework Design for DOAS, Ph.d., University of Mannheim, 2006.

Kulkarni, P., Baron, P., and Willeke, K.: Aerosol Measurement: Principles, Techniques, and Applications, Wiley, New York, 3 edn., 2005.

Liao, J., Sihler, H., Huey, L. G., Neuman, J. A., Tanner, D. J., Friess, U., Platt, U., Flocke, F. M., Orlando, J. J., Shepson, P. B., Beine, H. J., Weinheimer, A. J., Sjostedt, S. J., Nowak, J. B., Knapp, D. J., Staebler, R. M., Zheng, W., Sander, R., Hall, S. R., and Ullmann, K.: A comparison of Arctic BrO measurements by chemical ionization mass spectrometry and long path-differential optical absorption spectroscopy, Journal of Geophysical Research, 116, 1–14, doi:10.1029/2010JD014788, http://www.agu.org/pubs/crossref/2011/2010JD014788.shtml, 2011.

Liao, J., Huey, L. G., Tanner, D. J., Flocke, F. M., Orlando, J. J., Neuman, J. A., Nowak, J. B., Weinheimer, A. J., Hall, S. R., Smith, J. N., Fried, A., Staebler, R. M., Wang, Y., Koo, J.-H., Cantrell, C. a., Weibring, P., Walega, J., Knapp, D. J., Shepson, P. B., and Stephens, C. R.: Observations of inorganic bromine (HOBr, BrO, and Br 2) speciation at Barrow, Alaska, in spring 2009, Journal of Geophysical Research, 117, D00R16, doi:10.1029/2011JD016641, http://doi.wiley.com/10.1029/2011JD016641, 2012.

Peterson, P. K., Simpson, W. R., Pratt, K. A., Shepson, P. B., Frieß, U., Zielcke, J., Platt, U., Walsh, S. J., and Nghiem, S. V.: Dependence of the vertical distribution of bromine monoxide in the lower troposphere on meteorological factors such as wind speed and stability, Atmospheric Chemistry and Physics, 15, 2119–2137, doi:10.5194/acp-15-2119-2015, http://www.atmos-chem-phys.net/15/2119/2015/acp-15-2119-2015.html, 2015.

Platt, U. and Stutz, J.: Differential Optical Absorption Spectroscopy, vol. 90, Springer-Verlag Berlin Heidelberg, doi:10.1007/978-3-540-75776-4, http://www.springerlink.com/index/10.1007/978-3-540-75776-4, 2008.

Prados-Roman, C., Butz, A., Deutschmann, T., Dorf, M., Kritten, L., Minikin, A., Platt, U., Schlager, H., Sihler, H., Theys, N., Van Roozendael, M., Wagner, T., and Pfeilsticker, K.: Airborne DOAS limb measurements of tropospheric trace gas profiles: case studies on the profile retrieval of O4 and BrO, Atmospheric Measurement Techniques, 4, 1241–1260, doi:10.5194/amt-4-1241-2011, http://www.atmos-meas-tech.net/4/1241/2011/amt-4-1241-2011.html, 2011.

Rodgers, C. D.: Inverse Methods For Atmospheric Sounding: Theory and Practice, World Scientific, Singapore, 2000.

Rozanov, a., Rozanov, V., Buchwitz, M., Kokhanovsky, a., and Burrows, J. P.: SCIATRAN 2.0 - A new radiative transfer model for geophysical applications in the 175-2400 nm spectral region, Advances in Space Research, 36, 1015–1019, doi:10.1016/j.asr.2005.03.012, http://linkinghub.elsevier.com/retrieve/pii/S0273117705002887, 2005.

Tang, M. J., Cox, R. A., and Kalberer, M.: Compilation and evaluation of gas phase diffusion coefficients of reactive trace gases in the atmosphere: volume 1. Inorganic compounds, Atmospheric Chemistry and Physics, 14, 9233–9247, doi:10.5194/acp-14-9233-2014, http://www.atmos-chem-phys.net/14/9233/2014/, 2014.

Thompson, C. R., Shepson, P. B., Liao, J., Huey, L. G., Apel, E. C., Cantrell, C. A., Flocke, F., Orlando, J., Fried, A., Hall, S. R., Hornbrook, R. S., Knapp, D. J., Mauldin III, R. L., Montzka, D. D., Sive, B. C., Ullmann, K., Weibring, P., and Weinheimer, A.: Interactions of bromine, chlorine, and iodine photochemistry during ozone depletions in Barrow, Alaska, Atmospheric Chemistry and Physics, 15, 9651–9679, doi:10.5194/acp-15-9651-2015, http://www.atmos-chem-phys.net/15/9651/2015/acp-15-9651-2015.html, 2015.

Wachsmuth, M., Gäggeler, H. W., von Glasow, R., and Ammann, M.: Accommodation coefficient of HOBr on deliquescent sodium bromide aerosol particles, Atmospheric Chemistry and Physics, 2, 121–131, doi:10.5194/acp-2-121-2002, http://www.atmos-chem-phys.net/2/121/2002/, 2002.

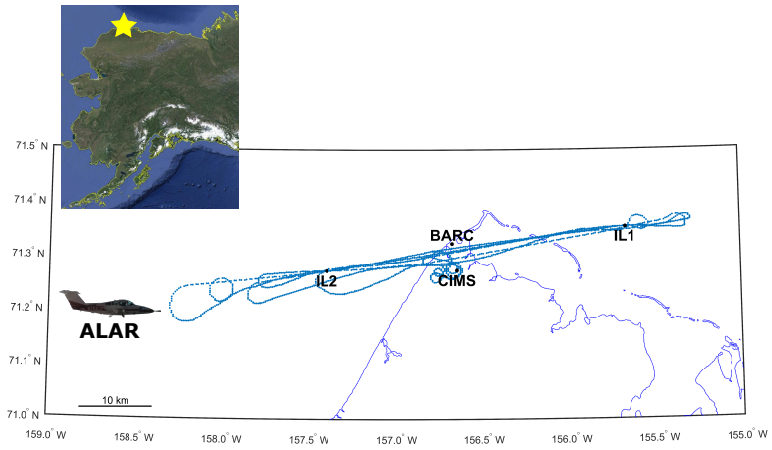

Figure S1. Location of ground based measurements with flight track overlaid. Locations of the Barrow MAX-DOAS instrument (BARC), the two icelanders (IL1 and IL2) as well as the location of the chemical ionization mass spectrometry measurements are shown. The location of Utqiaġvik (Barrow) is shown on the inset map of Alaska with a yellow star.

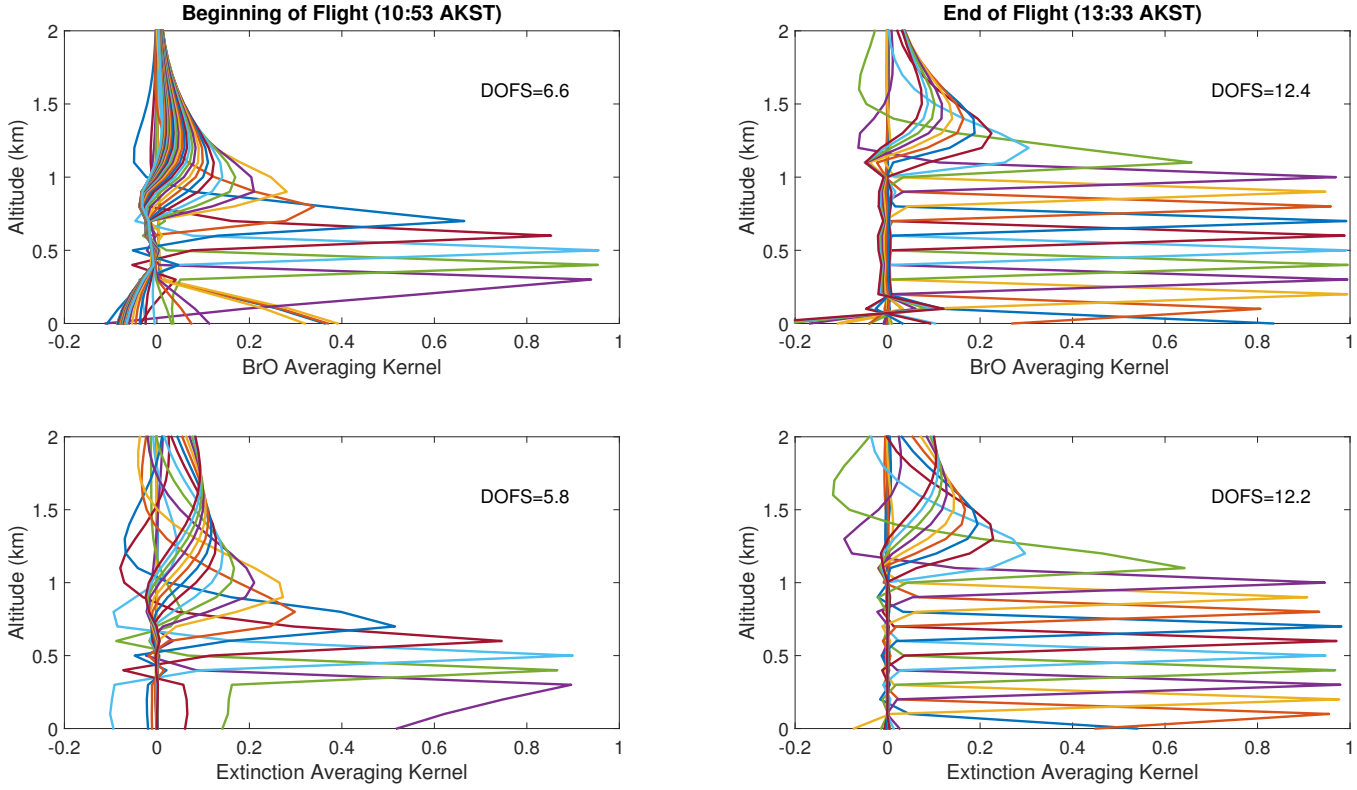

Figure S2. Averaging kernels and degrees of freedom for signal (DOFS) for the profile retrievals shown in main manuscropt Fig. 11.

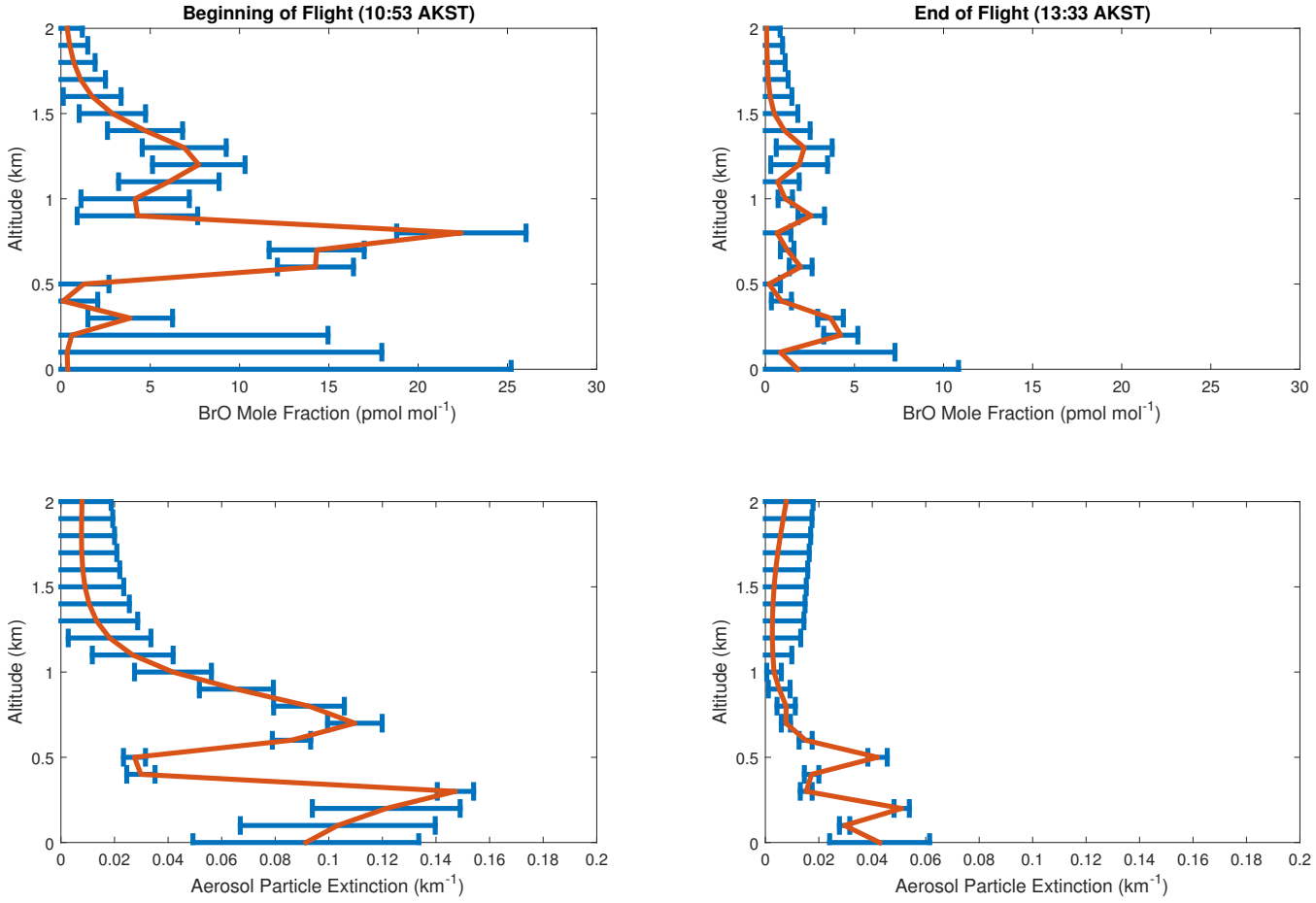

Figure S3. Retrieval errors for the profiles shown in main manuscript, Fig. 11.

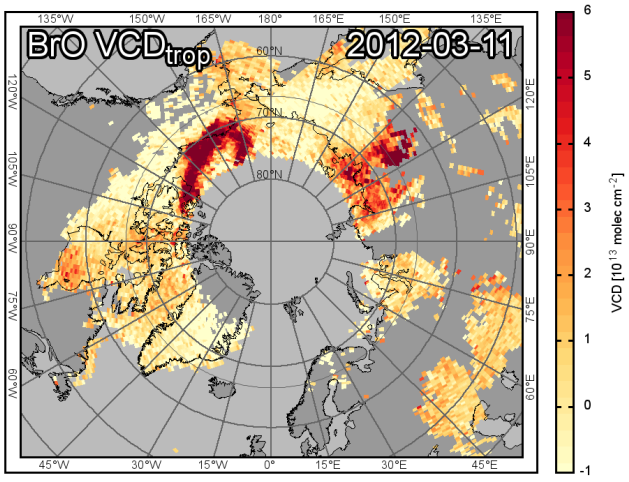

Figure S4. Pan-Arctic tropospheric BrO LT-VCDs on 11 March 2012 derived from GOME-2 spectra.

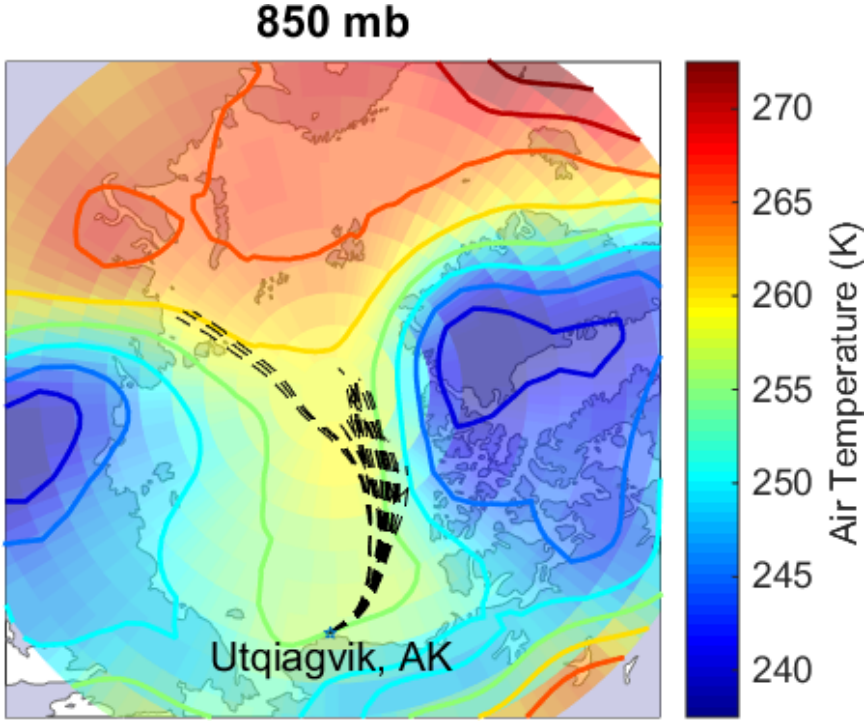

Figure S5. NOAA generated HYSPLIT backward air mass trajectories for the plume overlaid on daily averaged NCEP reanalysis data for 11 March 2012. All panels show an ensemble of 27 72 h trajectories. The ensemble is generated by offsetting the modeled meteorology used to calculate the trajectory by 1° horizontally and ∼250 m vertically prior to running HYSPLIT. NCEP Reanalysis data shows air temperature at 850 mb.

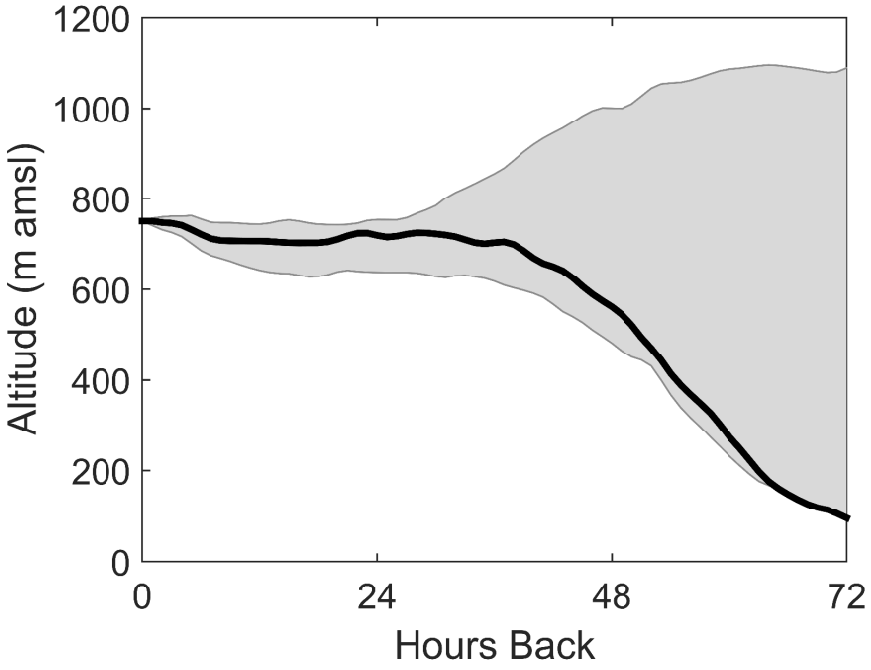

Figure S6. Vertical motion of the trajectories in Fig. S5. The trajectories are run 72 hours from the begining of the flight at Utqiavik, AK. The black line shows the modeled vertical motion, while the shaded region shown the uncertainty as modeled by running HYSPLIT in ensemble mode.

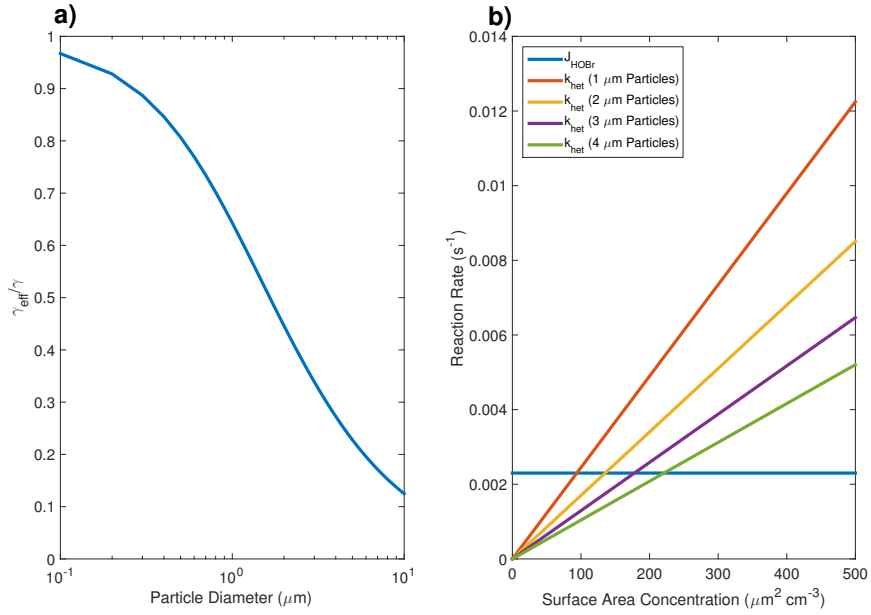

Figure S7. a) Calculated reduction ($\frac{\gamma_{eff}}{\gamma}$) of the aerosol uptake coefficient (γ) due to diffusion limitations. b) Calculated reaction rates for the heterogeneous reaction of HOBr with aerosol bromide to produce bromine compared to the photolysis rate of HOBr.